IOP PUBLISHING JOURNAL OF PHYSICS D: APPLIED PHYSICS

J. Phys. D: Appl. Phys. **45** (2012) 025303 (11pp) doi:10.1088/0022-3727/45/2/025303

Influence of the oxygen partial pressure and post-deposition annealing on the structure and optical properties of ZnO films grown by dc magnetron sputtering at room temperature

M Yuste, R Escobar Galindo, I Caretti, R Torres and O Sánchez

Instituto de Ciencia de Materiales de Madrid, Madrid, Spain

E-mail: rescobar@icmm.csic.es

Received 19 September 2011, in final form 18 November 2011
Published 20 December 2011
Online at stacks.iop.org/JPhysD/45/025303

Abstract

A systematic study for the optimization of the deposition process of ZnO thin films grown by dc magnetron sputtering at room temperature was carried out using different oxygen partial pressures and deposition times. We have established a correlation between the oxygen partial pressure, the chemical composition and the crystalline structure of the films.

Stoichiometric and highly oriented ZnO thin films along the (0 0 2) crystal plane with very good optical performance were obtained for a relative oxygen gas flow of 20% in the gas mixture. Higher O_2 concentrations resulted in non-stoichiometric ZnO with an excess of oxygen, which exhibited a lower degree of crystallinity and slightly higher band-gap energy.

X-ray absorption near edge structure (XANES) analysis indicated that this excess of oxygen was incorporated in molecular form inducing a reduction in the crystallinity of the material. Post-deposition annealing treatments up to 500 °C significantly improved their crystallinity as confirmed by x-ray diffraction and XANES. Therefore, it has been found that it is possible to grow ZnO at room temperature with high crystal quality and good optical response by controlling the growth conditions.

(Some figures may appear in colour only in the online journal)

1. Introduction

Transparent conductive oxides have been extensively studied for being one of the most important components for large area electronics devices such as solar cells, flat panel displays or optical sensors [1–3]. Zinc oxide possesses a unique position among these materials owing to its superior and diverse properties. ZnO is a transparent semiconductor of natural n-type conductivity with a direct band gap of 3.37 eV and large excitation binding energy (60 meV). Moreover, its optical behaviour (high transparency, near-UV emission and absorption), piezoelectricity, chemical stability, biocompatibility, high voltage–current nonlinearity, etc, have found many potential applications in the fabrication of microelectronic and optoelectronic devices such as thin film transistors (TFTs), ultraviolet resistive coatings, gas sensors, sonar and mobile phones [4–7]. In this sense, an advantage of zinc oxide over other materials is its low price, placing it as a highly potential candidate for outstanding industrial applications both as a transparent conductive oxide and as a semiconductor [8].

Recently, significant progress in ZnO crystal quality with hexagonal wurtzite structure and a strong tendency for self-organized growth has been made [9, 10]. In addition, nanostructures such as nanotubes, nanorods, nanowalls or nanofibers, high-quality undoped and doped ZnO thin films have also been grown [11–14]. Several techniques have been used for the fabrication of ZnO thin films, including chemical

vapour deposition, sol–gel, spray-pyrolysis, molecular beam epitaxy, pulsed laser deposition, vacuum arc deposition, sputtering and magnetron sputtering [15–18]. The latter is commonly used for the preparation of polycrystalline ZnO nanomaterials owing to the combined advantages of low deposition temperatures, reduced film damage, high deposition rates and compatibility with integrated circuit processing. Nevertheless, the energetic balance during film growth by magnetron sputtering is rather complicated. The flux of particles impinging the substrate consists mostly of low energy atoms (∼1 eV), gas ions of a few eV and some negative ions of much higher energy, typically a few 100 eV [19]. Depending on the experimental design of the magnetron sputtering system, this energy balance will change and, consequently, the properties of the films grown will be different. Therefore, despite the numerous research works carried out about the synthesis and properties of ZnO thin films grown by magnetron sputtering [20–23] it is difficult to find a systematic study about them.

Until now, mostly rf (radio frequency) magnetron sputtering has been used for the synthesis of ZnO obtaining high-quality ZnO thin films with a good *c*-axis orientation [24, 25]. However, the use of dc reactive magnetron sputtering has some advantages over rf magnetron sputtering, such as the possibility to grow ZnO films with tailored stoichiometries, a higher deposition rate and the lowest price for metal Zn targets as compared with ZnO targets (metal Zn targets are approximately three times cheaper than ZnO mixed targets).

Moreover, another advantage of the deposition by sputtering is the possibility of growing ZnO at room temperature, allowing the use of substrates that do not support high temperatures such as polymers and glasses [26, 27].

In this work, several ZnO thin films have been deposited by dc reactive magnetron sputtering at room temperature on single-crystal silicon substrates. We have established a correlation between the deposition parameters (relative O_2 gas flow and deposition time) and the final composition, microstructure (grain size and crystallinity) and optical properties (refractive index, n and optical band gap, E_g) of the films. In this way, stoichiometric ZnO samples with good optical and structural properties have been obtained. On the other hand, non-stoichiometric samples deposited with an excess of oxygen (non-stoichiometric oxygen) have been annealed, and the evolution of their properties with the post-deposition annealing treatments has been discussed.

2. Experimental details

ZnO films were grown by dc reactive magnetron sputtering on single-crystal silicon (1 0 0) wafers using a commercial zinc target of 99.99% purity, 3 inch diameter and 0.125 inch thickness. All experiments were performed introducing a mixture of Ar (99.999%) and O_2 (99.992%) gases in the vacuum chamber at a constant total gas flow (Ar + O_2) of 30 sccm (standard cubic centimetres per minute). The chamber was pumped out to a base pressure of 2×10^{-4} Pa and the working pressure was 3×10^{-1} Pa, approximately.

The silicon substrates were cleaned *ex situ* in consecutive ultrasonic baths of trichloroethylene, acetone, ethanol and distilled water. Prior to deposition, the target was pre-sputtered for 15 min to remove any impurity on its surface. To ensure that we were working under the reactive sputtering regime, the samples were grown after the total poisoning of the cathode. In all the deposition processes the target to substrate distance was kept at 13 cm and the cathode power was maintained at 100 W. Even though no intentional heating was applied to the substrate, a temperature between 90 and 100 °C was reached during deposition due to the impinging sputtered atoms.

Firstly, sputtering time was kept at 30 min while decreasing the relative O_2 gas flow (f_{O_2}) in the reactive atmosphere from 100 to 15%. Secondly, in order to minimize thickness effects, the sputtering time was adjusted to produce films with a constant thickness of approximately 200 nm for three f_{O_2}: 20%, 50% and 83%. The thickness of the films was measured using a mechanical stylus profilometer (Veeco Dektak 150).

For the study of the chemical composition of the ZnO films, Rutherford backscattering spectroscopy (RBS) experiments were carried out with the 5 MV HVEE Tandetron accelerator sited at the Centro de Micro-Análisis de Materiales of Universidad Autónoma de Madrid [28]. The RBS experiments were performed using 3.035 MeV He^+ ions to make use of the cross-section resonance ^{16}O (α, α) ^{16}O at that particular energy and, therefore, to improve the sensitivity to oxygen. The chemical composition of the ZnO films has been extracted using the RBX software [29].

The films' crystalline structure was determined by x-ray diffraction (XRD) using a Cu anode (Cu K_α = 1.54 Å) working under grazing incidence conditions (angle of incidence 0.7°) at room temperature. The XRD measurements were performed on a Siemens D-5000 diffractometer.

The surface and fracture cross-section morphologies of the thin films were examined by a Nova NanoSEM 230 FEI scanning electron microscope (SEM).

In selected samples, we studied the bonding structure and phase composition by x-ray absorption near edge structure (XANES) analysis. These measurements were done at the PM4 beamline of the Bessy II synchrotron facility (Berlin, Germany), using the SurICat endstation. The XANES spectra were recorded in the total electron yield (TEY) mode by registering the current drained to ground from the sample. The latter was normalized to the current from a gold-coated grid located upstream in the x-ray beam path.

Spectroscopic ellipsometry (SE) was used to determine the optical properties (refractive index n, and extinction coefficient, k) in the visible range. Measurements were performed on a M-2000U ellipsometer working in the 250–1600 nm range and an incidence angle of 70°. The CompleteEASE 4.06 software was used to analyse the ellipsometric data [30]. The optical energy gap E_g was derived from SE assuming a direct type transition. Post-deposition annealing treatments were carried out in vacuum ($P = 4 \times 10^{-3}$ Pa) for 30 min at 400 and 500 °C in a resistive furnace with a heating rate fixed at 4 °C min^{-1}.

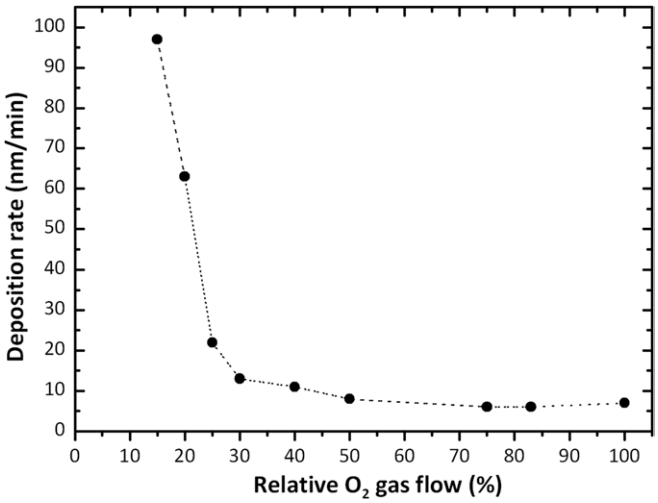

Figure 1. Variation of the deposition rate as a function of the relative oxygen gas flow. The error in the deposition rate is inside the symbols.

3. Results and discussion

3.1. Optimization of growth parameters for ZnO thin films

ZnO thin films were deposited using different relative O_2 gas flows in the reactive mixture (15–100%) for a constant deposition time of 30 min. In this way, the thickness of the layers varied between 170 and 3000 nm, approximately. The deposition rate shown in figure 1, abruptly decreases from 97 to 13 nm min^{-1} up to a relative O_2 flow of 30%, and then it stays fairly constant at a value of (8 ± 2) nm min^{-1} for higher O_2 partial pressures (the oxygen partial pressure was considered to be the concentration percentage of the O_2 introduced in the total flow gas).

The two typical regimes of a sputtering process [31] are clearly differentiated from figure 1: (i) a metallic regime with high deposition rates for low f_{O_2} (<30%) and (ii) a reactive regime with lower deposition rates for high f_{O_2} (>30%). An extensive chemical, structural and optical characterization of these ZnO films has been consequently carried out.

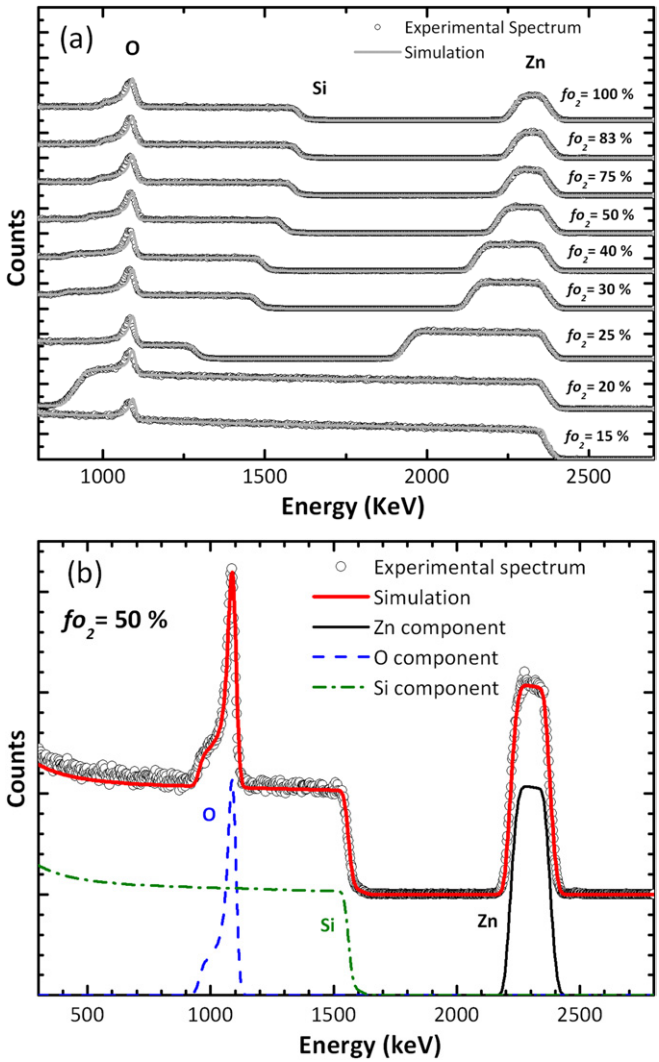

Figure 2. RBS collected spectra at the 3.035 MeV oxygen resonance for ZnO samples grown during 30 min. (*a*) RBS experimental data and global fitting of results for samples deposited at f_{O_2} = 15–100%. (*b*) Elemental components extracted with RBX simulations from the original experimental spectrum for a deposited sample at f_{O_2} = 50%.

3.1.1. Chemical composition. Figure 2(*a*) displays the RBS spectra (experimental data and the global fit results) of the ZnO films deposited at different oxygen partial pressures. For the particular case of a film deposited at $f_{O_2} = 50\%$ (also applicable to the other samples), figure 2(*b*) shows three different components that can be extracted from the experimental data fitting: Zn and O belonging to the film and Si from the substrate.

The RBX simulations were carried out assuming a single ZnO layer on silicon substrate and considering the ZnO layer thickness measured by profilometry. A very precise fitting was obtained without an interfacial layer between the ZnO film and substrate. This indicates that deposited films were homogeneous along the thickness with an abrupt interface. The above-mentioned differences in the deposition rate are clearly observed in the RBS spectra of figure 2(*a*). The Zn signal narrows as the O_2 partial pressure increases for a constant deposition time of 30 min, indicating a decrease in the ZnO thickness. In order to avoid the effect of thickness variation and to isolate the effect of the oxygen partial pressure (as discussed in section 3.1.2), ZnO coatings with a fixed thickness close to 200 nm have also been grown using three different f_{O_2} (20%, 50% and 83%). In table 1 a summary of the chemical composition (and optical properties discussed in section 3.1.3.) of the deposited samples is shown. Comparing theses samples with the 200 nm thick ones presented in section 3.1.2, it is clear that the thickness of the films does not affect their chemical composition. The RBX analysis, together with profilometry thickness measurements, was also used to estimate the density (ρ) of the deposited films (see table 1).

Note that the density values obtained are close to the reference value for ZnO (5.6 g cm^{-3}) [32]. In particular, the samples grown at $f_{O_2} = 20\%$ have the same density as the reference. In figure 3 the variation of the ZnO films' composition with the oxygen partial pressures used during the growth process is shown.

Table 1. Summary of the chemical composition, density and optical properties of the ZnO samples. The error in the composition and density was estimated to be of ±1 at% and ±0.1 g cm^{-3}, respectively.

f_{O_2} (%)	Thickness (nm)	Zn (at%)	O (at%)	Density, ρ (g cm^{-3})	n, 600 nm	E_g (eV)
15	2945 ± 55	56	44	4.8	1.61	[a]
20	1457 ± 40	47	53	5.6	1.99	3.31
	200 ± 4	46	54	5.6	2.00	3.31
25	639 ± 13	45	55	5.4	2.02	3.41
30	361 ± 6	45	55	5.4	1.99	3.42
40	335 ± 4	45	55	5.4	2.02	3.41
50	231 ± 5	43	57	5.4	1.97	3.42
75	197 ± 13	43	57	5.4	2.04	3.42
83	173 ± 4	43	57	5.4	2.02	3.42
	190 ± 10	43	57	5.4	2.05	3.43
100	167 ± 3	41	59	5.4	1.99	3.41
ZnO reference				5.6 [32]	2.03 [33]	3.37 [34]

[a] Due to the metallic character of this sample, no E_g was measured.

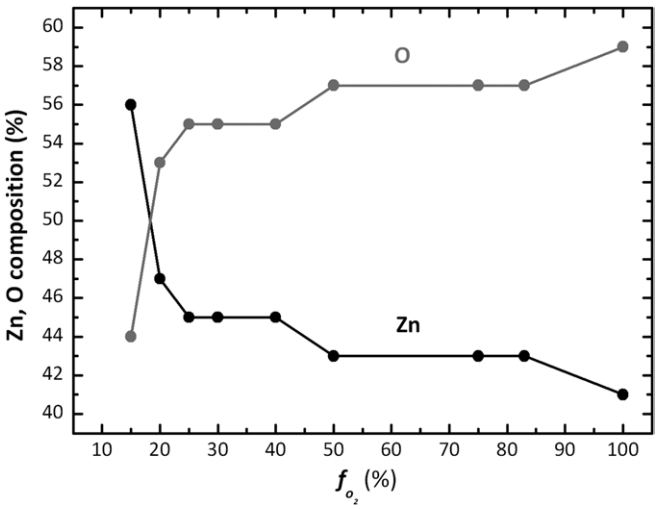

Figure 3. ZnO layers composition obtained from RBS measurements.

The oxygen content in the films increases with the O_2 partial pressure. The most metallic like films with a 56 at% of zinc content are obtained for the lowest O_2 gas concentration (15%). Applying a mixture rule, the amount of metallic Zn in the film can be estimated to be of approximately 15 at%. For $f_{O_2} = 20\%$ the most stoichiometric ZnO is obtained (Zn/O = 47/53) whilst for higher O_2 concentrations (up to 83%) the chemical composition of the ZnO layers is almost constant at Zn/O = 44/56. The sample grown with $f_{O_2} = 100\%$ presents the lowest Zn at% content because it was deposited with no argon in the total gas flow. Therefore, for $f_{O_2} > 20\%$, an oxygen excess of more than 5 at% is detected by RBS with respect to stoichiometric ZnO. This additional oxygen might be incorporated either (i) in the ZnO lattice as interstitial atoms or at Zn sites or (ii) out of the lattice being absorbed on the surface or embedded as molecular oxygen (O_2). In any case, the presence of additional non-stoichiometric oxygen in the films will entail a stress of the ZnO lattice. This will be discussed later (in section 3.2) in more detail from XRD results

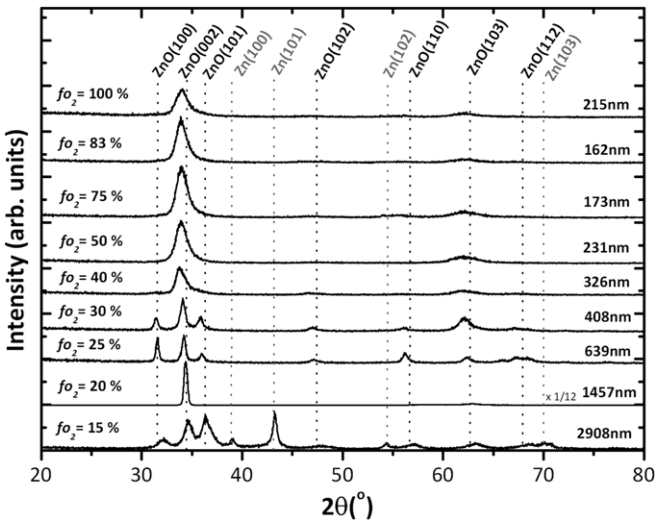

Figure 4. XRD pattern of ZnO films grown at different relative oxygen gas flows and a fixed deposition time of 30 min.

and in connection with the XANES analysis of post-deposition annealed samples.

3.1.2. Structural properties. The XRD patterns of the ZnO films deposited at different oxygen partial pressures and a fixed deposition time of 30 min are shown in figure 4.

The XRD spectra revealed that the grown ZnO films were crystalline with a wurtzite structure (w-ZnO) (JCPDS card No 36-1451) [35]. Only for the sample with the highest Zn content deposited using $f_{O_2} = 15\%$, both wurtzite ZnO and metallic zinc (JCPDS card No 40831) structures were simultaneously present.

In general, a higher degree of polycrystallinity was observed for samples grown with low f_{O_2} between 15% and 30%, except for the film grown with $f_{O_2} = 20\%$ due to thickness effects at this relative oxygen gas concentration (discussed below). For samples deposited with higher f_{O_2} (40–100%) we detected a more monocrystalline structure, as confirmed by the presence of a dominant and very intense (0 0 2) diffraction peak in the XRD patterns. This indicates a preferential orientation with the c-axis perpendicular to the substrate surface. We ascribed the changes observed in the crystallinity to the size of the ZnO particles formed during the deposition process. When the relative oxygen gas flow is high and the amount of Ar particles in the plasma is low, the Zn particles sputtered from the target and the ZnO grains deposited on the substrate are small being easy to orientate in one direction entailing a monocrystalline ZnO [24].

To disclose thickness effects on the ZnO structure for a fixed oxygen concentration in the gas mixture, we have followed the evolution of the diffraction peaks of samples deposited with $f_{O_2} = 20\%$ and thicknesses ranging from 100 to 1925 nm (see figure 5(a)).

From the XRD pattern, we have calculated the grain size from the (0 0 2) orientation according to Scherrer's formula [36], the internal stress σ, derived from the change in the 'c' lattice parameter [37] and the film texture (defined as the $I_{(002)}/I_{(103)}$ ratio between the intensities of (0 0 2) and

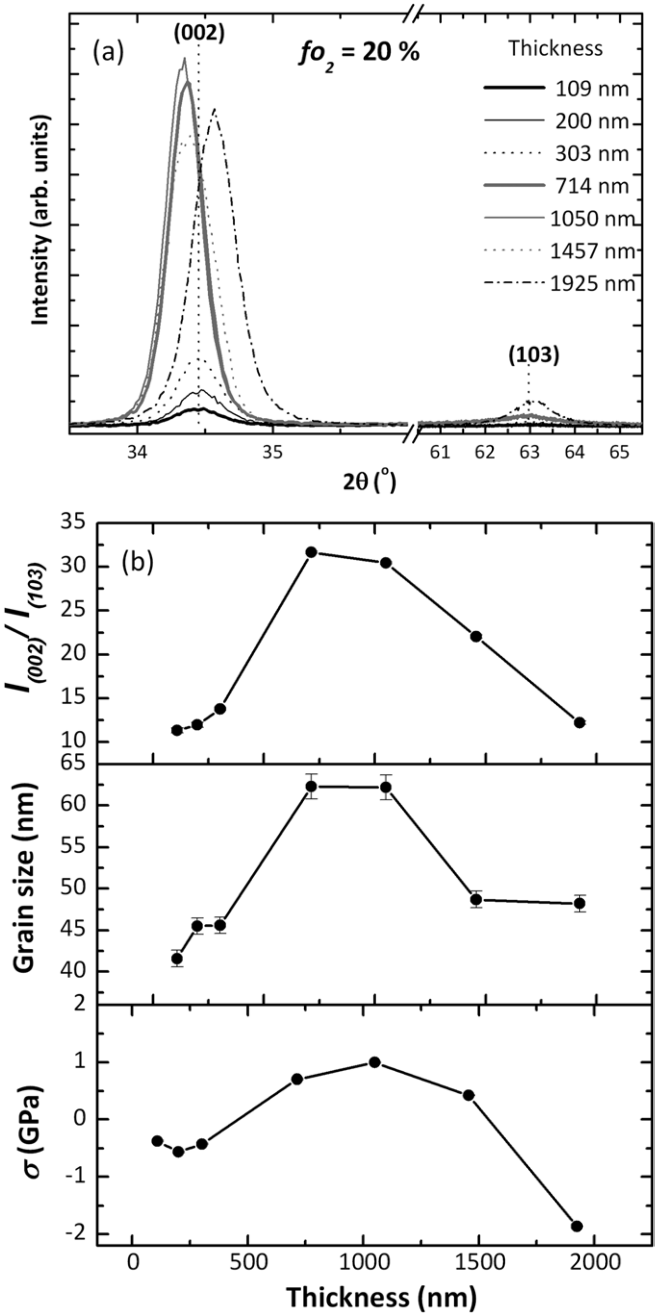

Figure 5. (*a*) XRD pattern of ZnO films grown at $f_{O_2} = 20\%$ with a thicknesses range from 100 to 1925 nm. (*b*) Variation of the intensity ratio (0 0 2)/(1 0 3), the grain size and the internal stress with the thickness for ZnO grown at $f_{O_2} = 20\%$. The errors in the intensity ratio (0 0 2)/(1 0 3) and in the internal stress lie inside the symbols.

(1 0 3) orientations) [38] (see figure 5(*b*)). Initially, for samples below 300 nm thick, the ratio $I_{(0\,0\,2)}/I_{(1\,0\,3)}$ remains lower than 15 presenting a state of compressive stress ($\sigma < 0$) with grain sizes smaller than 46 nm. With the increase in the ZnO thickness (up to ∼1000 nm), the stress changes from compressive to tensile ($\sigma > 0$), the $I_{(0\,0\,2)}/I_{(1\,0\,3)}$ ratio rises up to 30 and a marked preferential orientation of the films is observed resulting in the highest grain size (∼62 nm). Finally for samples with thickness above 1000 nm, the residual stress, the texturization and the grain size monotonically decrease and for the particular case of the thickest sample (1925 nm)

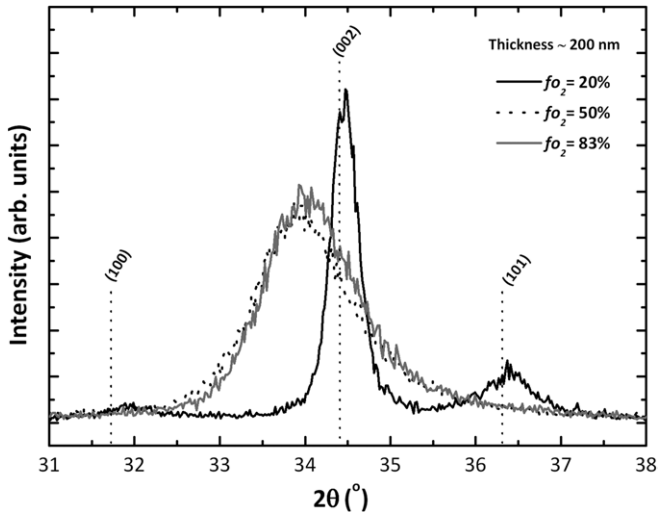

Figure 6. XRD pattern of 200 nm ZnO films grown at $f_{O_2} = 20\%$, 50% and 83%.

the internal stress returns again to a compressive state. In view of these results, we can conclude that the grain size, the texture and the stress of the samples are determined by the thickness. In particular, the evolution of the stress with the film thickness (from compressive to tensile, and then again to compressive stress) can be explained in terms of a mechanism of stress generation and relaxation during coalescence as Floro *et al* showed in their work [39].

Now, in order to determine solely the influence of the oxygen partial pressure we proceeded to deposit films at different f_{O_2} (20%, 50% and 83%) with a fixed thickness of 200 nm (see figure 6).

The three 200 nm ZnO thin films grew with (0 0 2) preferential orientation, but the film deposited with $f_{O_2} = 20\%$ presented a narrower and more intense (0 0 2) reflection at the position corresponding to the ZnO reference. Moreover, two extra peaks corresponding to (1 0 0) and (1 0 1) orientations are also detected, which are not observed for the samples grown with $f_{O_2} = 50\%$ and 83%. This confirms our preliminary observation that for a constant thickness, the polycrystallinity of the films decreases with increasing the relative oxygen gas flow.

Regarding the stress, as we increase the O_2 partial pressure, the position of the (0 0 2) orientation appears shifted to lower angles with respect to the value for a ZnO bulk crystal. This again points to a residual compressive stress, although its source cannot be ascribed in this case to the thickness of the films, as occurred for the thicker samples in figure 4(*a*). In contrast, this stress observed in the 200 nm thick layers grown with $f_{O_2} = 50\%$ and 83% is due to the formation of crystallite imperfections during growth. The formation of these defects depends, among other deposition factors, on the incorporation of additional oxygen [40]. The RBS results already suggested the presence of such non-stoichiometric oxygen in the samples. In fact, it is worth noting that the crystallinity of the films, determined from the grain size and the *d*-spacing values, improves at low oxygen partial pressures. The values obtained for the grain size were 51 nm, 14 nm and

14 nm for the 200 nm thick samples deposited at 20%, 50% and 83% relative O_2 gas flows, respectively. The d-spacings, calculated from Braggs's law, were 2.60, 2.64 and 2.63 Å, respectively (d-spacing$_{ZnO}$ = 2.6032 Å [40]).

Regarding the morphology of the samples, a transversal SEM view of a ZnO film deposited at an intermediate f_{O_2} (50%) is shown in figure 7(a).

The ZnO film has a uniform structure with the crystalline growth parallel to the c-axis. A columnar structure throughout the film thickness is clearly visible. The low temperature during the film growth (∼100 °C), associated with low bombardment conditions, promotes the development of this kind of structure, due to the low adatom mobility as described by Movchan and Demchishin [41] and Thornton [42]. The rest of the samples grown at different O_2 partial pressures show the same columnar structure. The influence of the oxygen partial pressure in the surface morphology of 200 nm thick ZnO films can be appreciated in the surface SEM images of figure 7. Histograms of the column width distribution are also included as insets. The histograms indicate that the sample deposited with less oxygen (20%) has a more heterogeneous distribution of wider columns (37 ± 13 nm). In contrast, the film deposited with more oxygen (83%) presents a more homogeneous distribution of narrower columns (23 ± 4 nm). Therefore, there is a correlation between the grain size and the column width of the ZnO films obtaining higher values using low relative oxygen gas flow.

In view of the above-mentioned results, it is concluded that the best crystalline quality (by means of texture, grain size and d-spacing closed to the reference value) is obtained for films deposited at f_{O_2} = 20% with thicknesses above 300 nm.

3.1.3. Optical properties. The refractive index (n) and extinction coefficient (k) of the samples have been obtained by spectroscopic ellipsometry. The values of n and k were calculated using a Cauchy model suitable for semiconductor materials from the experimental data (ψ and Δ, which describe the polarization state of the light reflected off the surface of the film). To define n and k, the following formulae were used [43]:

$$n(\lambda) = A + \frac{B}{\lambda^2} + \frac{C}{\lambda^4}, \tag{1}$$

$$k(\lambda) = \alpha e^{12400\beta(1/\lambda - 1/\gamma)}. \tag{2}$$

where λ (wavelength) is in nm and A, B, C, α (coefficient amplitude), β (exponent factor) and γ (band edge) are fitting parameters. The energy band gaps were estimated assuming a direct type transition [44] from equations (2) and (3) [45]:

$$(\alpha h\nu)^2 = A(h\nu - E_g), \tag{3}$$

$$\alpha = \frac{4\pi k}{\lambda}, \tag{4}$$

where A is a constant, E_g is the optical energy band gap and α is the optical absorption coefficient that can be calculated from the k of SE results. The optical band gap E_g can then be obtained from the intercept of $(\alpha h\nu)^2$ versus $h\nu$ for direct allowed transitions [46]. The n and E_g values obtained are

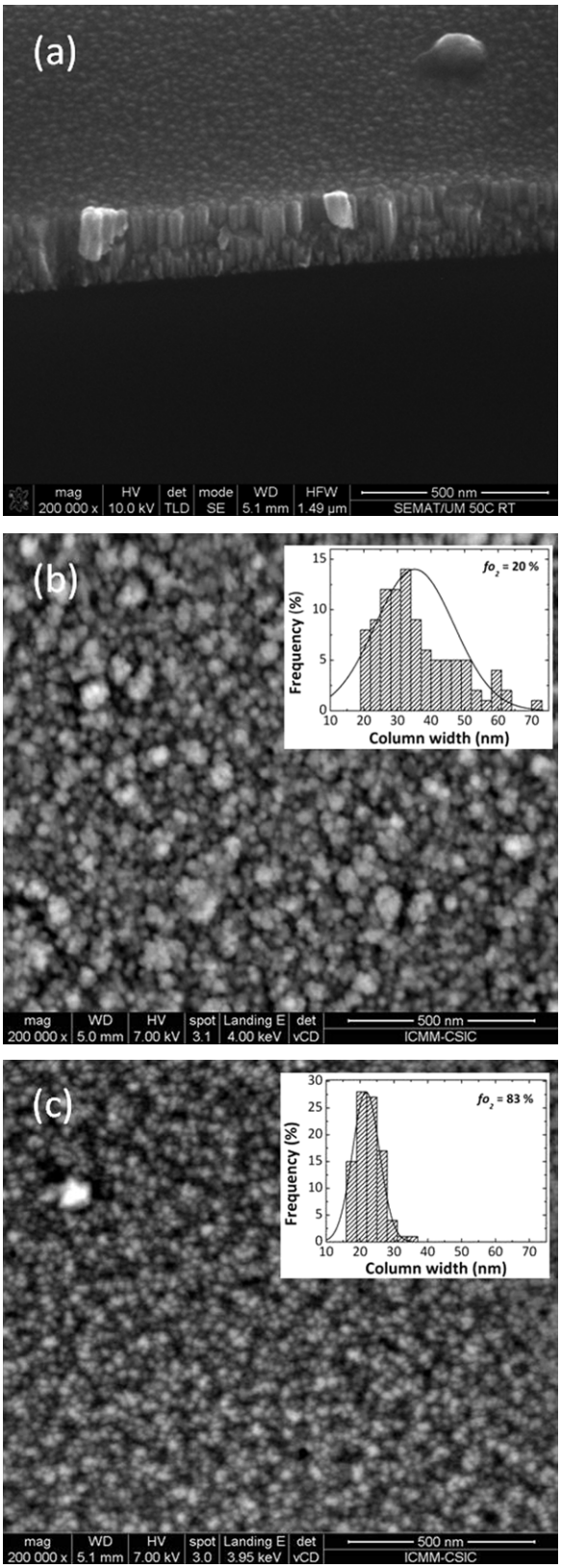

Figure 7. (a) Transversal SEM image of a ZnO film deposited at f_{O_2} = 50%. Surface SEM images of 200 nm ZnO films deposited at f_{O_2} = 20% (b) and 83% (c). The inset figures show the histogram of the column widh distribution.

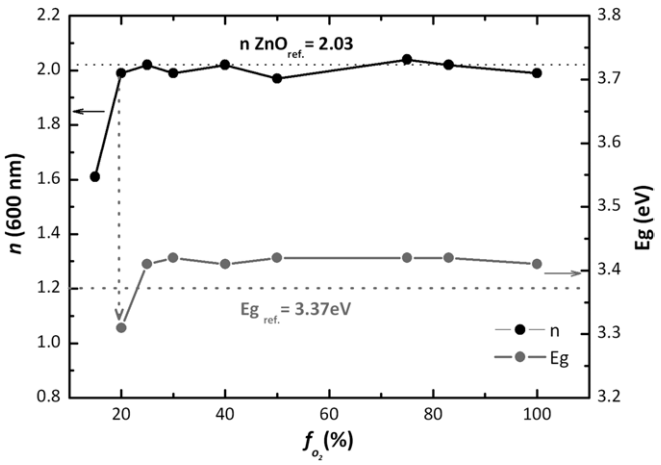

Figure 8. Variation of the refractive index n at 600 nm, and the optical energy band gap E_g, calculated from ellipsometric measurements, with the relative oxygen gas flow. In dotted line, reference values for ZnO [32, 33].

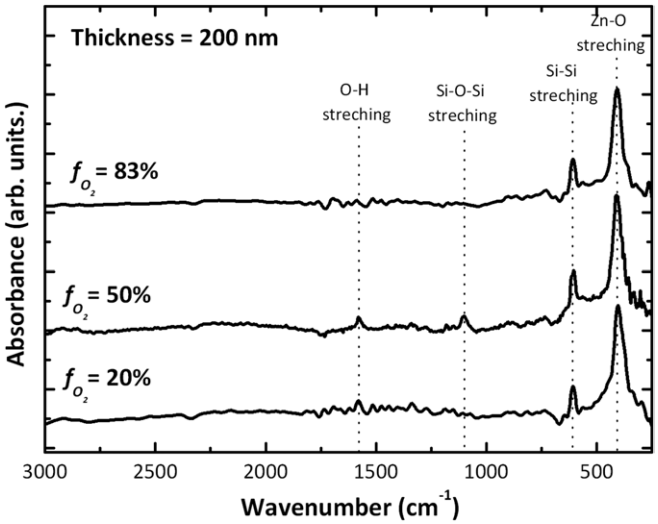

Figure 9. Infrared absorption spectra of 200 nm-thick ZnO films grown at $f_{O_2} = 20\%$, 50% and 83%.

presented in table 1 and figure 8 shows the variation of n (left axis) and E_g (right axis) with the relative O_2 gas flow.

At 600 nm the refractive index of the deposited samples is close to the reference value ($n_{ZnO} = 2.03$) [33], except for the sample deposited at $f_{O_2} = 15\%$ for which the refractive index tends to the metallic zinc refractive index ($n_{Zn} = 1.002$) [32]. This fact can be explained by the metallic character of the ZnO coating deposited at the lowest O_2 partial pressure. The sample deposited at $f_{O_2} = 20\%$ presents an E_g of 3.31 eV, slightly below the reference value ($E_{gZnO} = 3.37$ eV) [34], while samples grown with high f_{O_2} were found to have higher E_g values (3.41 ± 0.01 eV). This behaviour is in agreement with the work by Tan *et al* [47] showing that a decrease of the crystallinity entails an optical band gap shift to higher energies. It is worth noting that the optical properties of the films are independent of the thickness for a fixed partial pressure of oxygen (i.e. samples grown at $f_{O_2} = 20\%$ and thicknesses of 1457 and 200 nm). Hence, it is mainly the oxygen partial pressure which will determine the final optical characteristics of the ZnO material prepared.

3.1.4. Chemical environment. Figure 9 shows the IR spectra of the 200 nm ZnO films deposited at 20%, 50% and 83% of relative oxygen gas flow in the spectral range 3000–250 cm^{-1}.

In this spectral range, the very weak absorption bands located at 1578 and 1100 cm^{-1} are assigned to the existence of hydroxyl groups [48] on the surface of the samples and to the native SiO_2 of the silicon substrates [49], respectively. These vibration modes are mainly observed for the sample grown with a 50% of f_{O_2}. The absorption at 608 cm^{-1} corresponds to the Si–Si stretching from the substrate [50]. The only absorption band associated with Zn–O bonds appears at 410 cm^{-1} [48]. Thus, the same chemical environment is observed by IR absorption in all the 200 nm thick samples investigated. Similar results were obtained for thicker samples. More information about the chemical environment was obtained by XANES and the results will be presented in section 3.2. Anticipating the results, we mainly observed changes in the O K-edges XANES spectra of the ZnO samples deposited with higher oxygen flows (50% and 83%) where an excess of oxygen content was detected.

In this first part of the research we have established a correlation between the oxygen partial pressure, the chemical composition, the structural and optical properties and the chemical environment of the ZnO films. As a whole, it is possible to obtain ZnO thin films by dc reactive magnetron sputtering at room temperature with a controlled stoichiometry and optical properties similar to bulk ZnO. Regarding crystalline properties, ZnO films present wurtzite structure and columnar growth with the (0 0 2) preferential orientation. It has been observed that samples deposited at low oxygen partial pressure ($f_{O_2} = 20\%$) have a chemical composition very close to stoichiometric ZnO. Furthermore, they present the best crystal quality, higher grain size and denser morphology. In contrast, samples deposited at higher oxygen partial pressures ($f_{O_2} = 50$ and 83%) were found to have an excess of oxygen atomic content and less crystal quality in terms of grain size and d-spacing. Therefore, in the second part of this work, post-deposition annealing treatments were done on these samples that present an excess of oxygen in order to (i) improve their quality, (ii) study the changes that high temperatures produce in the ZnO properties and (iii) establish a correlation between these changes and the bonding structure by XANES analysis.

3.2. Post-deposition annealing treatments

Post-deposition annealing treatments at 400 and 500 °C during 30 min were done on samples deposited at room temperature with $f_{O_2} = 50\%$ and 83%.

The chemical composition and the optical properties of the annealed samples were measured by RBS and SE, and the obtained results are shown in table 2 together with the as-deposited samples.

Changes in the stoichiometry of the samples have been observed detecting a slight loss of oxygen after heating which is

Table 2. Summary of the chemical composition, density and optical properties of 200 nm-thick ZnO films as deposited and annealed at 400 and 500 °C. The error in the composition and density was estimated to be of ±1 at% and ±0.1 g cm^{-3}, respectively.

f_{O_2} (%)	Annealing temperature (°C)	Chemical composition		Density, ρ (g cm^{-3})	n, 600 nm	E_g (eV)
		Zn (at%)	O (at%)			
20	As deposited	46	54	5.6	2.00	3.31
50	As deposited	43	57	5.4	1.97	3.42
	400	45	55	5.4	1.99	3.41
	500	45	55	5.4	1.97	3.41
83	As deposited	43	57	5.4	2.05	3.43
	400	45	55	5.4	2.05	3.41
	500	45	55	5.4	1.98	3.41
ZnO reference				5.6 [32]	2.03 [33]	3.37 [34]

plausible to be ascribed to the desorption of molecular oxygen. These small changes are, however, higher than the error of the measurement and they have been confirmed by elastic recoil detection analysis (not presented in this paper). The annealed samples presented a composition similar to the samples with the best crystallinity (deposited at $f_{O_2} = 20\%$) while the thickness and the density of the films did not vary. Regarding n and E_g, they did not present significant changes after annealing treatments.

The XRD analyses of the treated samples are shown in figure 10 and compared with their as-deposited diffraction spectra.

Changes in the intensity and position of the preferential (0 0 2) diffraction are clearly observed. On the one hand, the highest crystallinity was obtained after post-annealing at 400 °C and 500 °C for samples deposited at $f_{O_2} = 50\%$ and $f_{O_2} = 83\%$, respectively. On the other hand, a shift of the (0 0 2) diffraction peak to higher 2θ angles was detected after annealing for the two samples. This shift indicates a shorter (0 0 2) interplanar distance. Therefore, the annealing at 400 and 500 °C of the samples grown at $f_{O_2} = 50\%$ and 83% entailed a relaxation of the stress and the improvement of crystal quality. This behaviour has also been observed in other reported works [37, 40].

The bonding structure of these samples, for which the change in crystallinity is most noticeable, was investigated by XANES before and after the annealing, and in comparison with the most crystalline as-deposited sample ($f_{O_2} = 20\%$). The corresponding Zn $L_{3,2}$- and O K-edge XANES spectra are depicted in figure 11, together with a $w-$ZnO reference taken from [51].

The Zn $L_{3,2}$-edge XANES spectra are typical of a w-ZnO material (see reference spectrum in dotted line), with no significant differences between the deposited ZnO samples. Only some minor intensity changes were visible in the L_3-edge features linked to Zn $2p_{3/2} \rightarrow$ 4s/d transitions, which will be discussed later in more detail. Regarding the O K-edge XANES spectra, states between ~530–539 eV are mainly attributed to O 2p–Zn 4s hybridization in ZnO [52, 53]. Polarization studies and theoretical calculations have confirmed that the sharp peak at ~537 eV corresponds to transitions to O $2p_z$ and O $2p_{x+y}$ states [54]. For photon energies higher than ~539 eV, mainly transitions to O 2p states hybridize with Zn 4pd states are detected [52, 53]. Interestingly, a narrow peak (labelled as A) was clearly visible

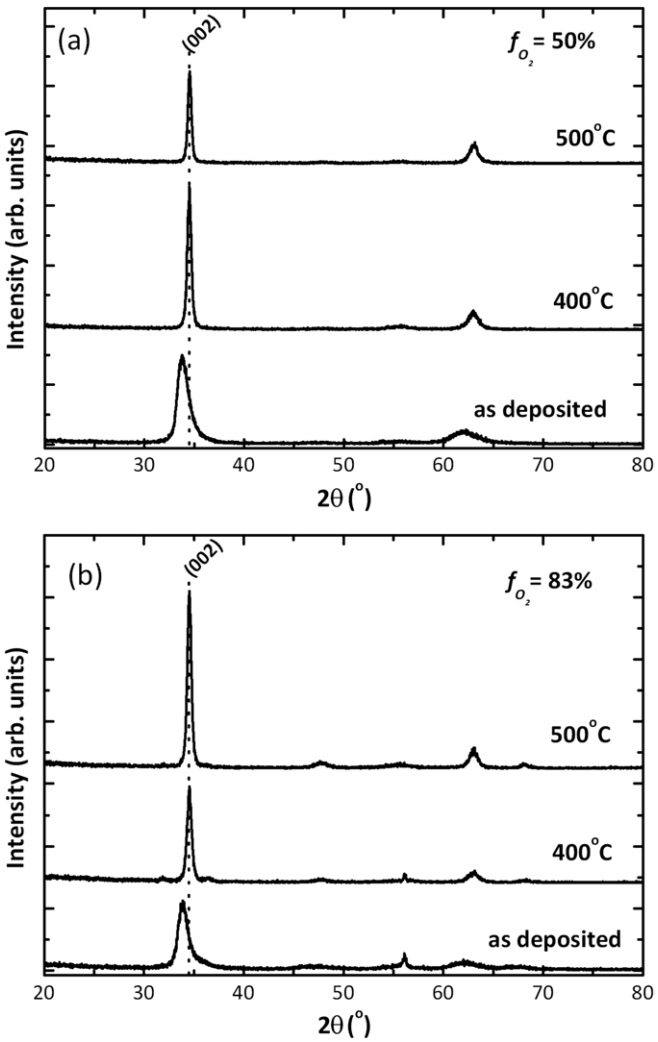

Figure 10. XRD pattern of ZnO films deposited at $f_{O_2} = 50\%$ (*a*) and $f_{O_2} = 83\%$ (*b*) post-annealed at 400 and 500 °C with their as-deposited spectra.

at 532.7 eV, which was absent in the oxygen spectrum of the ZnO reference. This peak has previously been ascribed to an increase in the density of unoccupied 3d states due to metal doping [52, 55], in agreement with theoretical calculations [56, 57]. However, in the case of pure ZnO, where no accessible empty 3d states are present, this peak was linked in previous studies to defects in the ZnO crystalline structure, such as O vacancies [52]. In this sense, note that peak A is

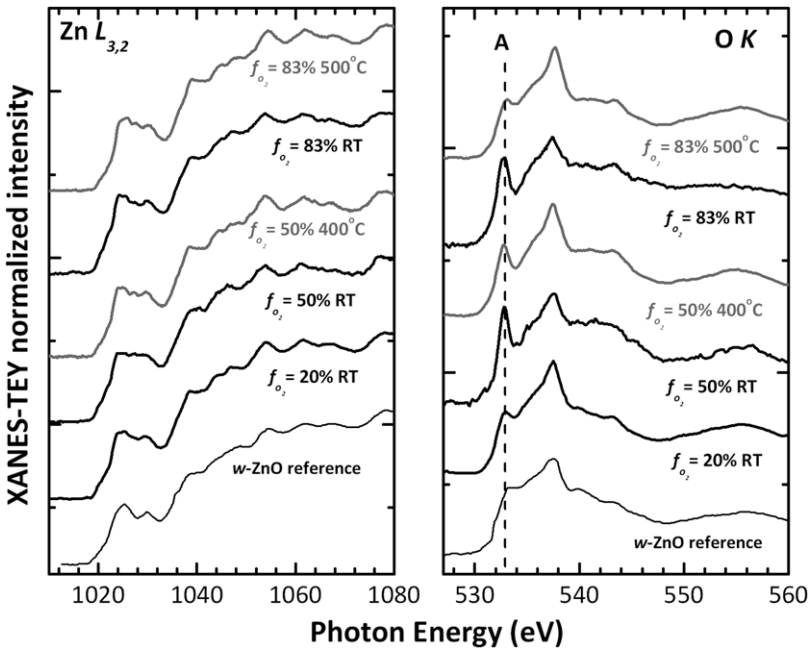

Figure 11. Zn $L_{3,2}$- and O K-edge XANES spectra of ZnO films grown at different relative oxygen gas flows at room temperature (black curves) and after the post-annealing treatment (grey curves). The reference spectra of w-ZnO are shown for comparison purposes [51].

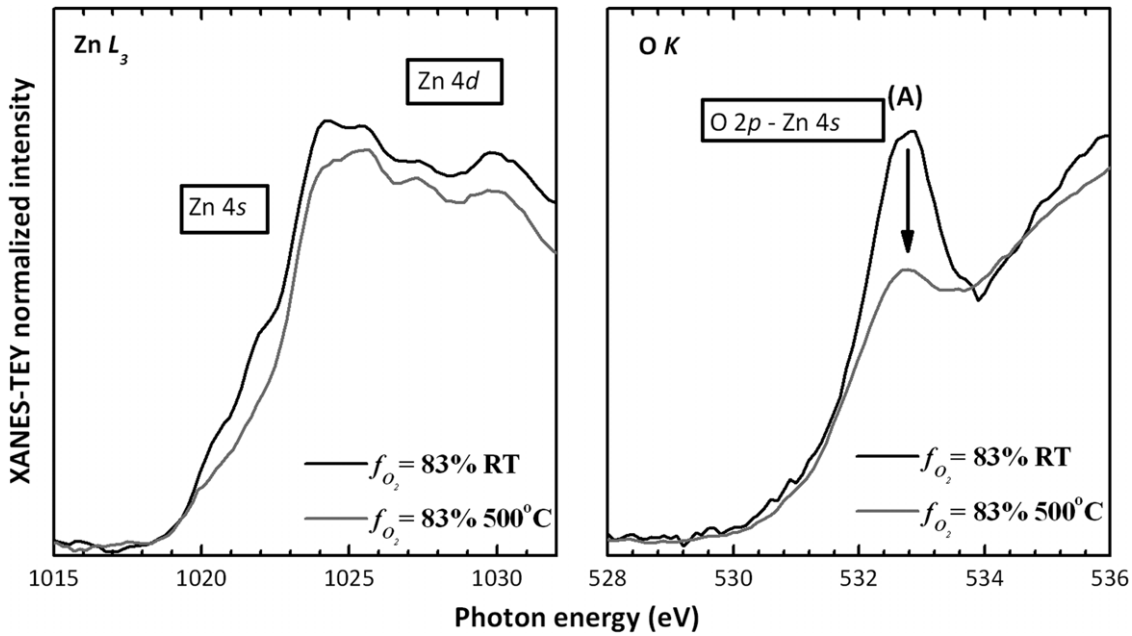

Figure 12. Zn L_3- and O K- edge XANES spectra enlarged.

hardly observable in the ZnO deposited at $f_{O_2} = 20\%$, which has the most stoichiometric composition and the best crystal quality, but is apparent in samples grown at $f_{O_2} = 50\%$ and 83% with an excess of oxygen content and lower crystallinity. Moreover, when the latter are annealed at 400 and 500 °C a decrease in the intensity of peak A was detected. Thus, peak A is clearly related to the degree of crystallinity of the material. Interestingly, peaks at similar energies have been reported for molecular O adsorbed on metal surfaces [58, 59]. Since the synthesis was carried out in oxygen atmosphere, we tentatively assign peak A to incorporation of non-reacted molecular oxygen in the ZnO films. An analogous effect has been observed during the growth of N-based coatings by PVD methods, where part of the nitrogen was incorporated in molecular form [60]. These results suggest that the excess of oxygen observed for the less crystalline samples with respect to a ZnO stoichiometry (see RBS results) is assimilated as molecular oxygen, which reduces the crystal periodicity by inducing lattice defects.

As reflected in figure 12, the higher the intensity of peak *A* the larger the density of Zn 4s and 4d states due to the presence of defects.

Crystallization of the ZnO sample after annealing is, therefore, followed by a clear decrease of peak A and a decrease in the Zn L_3-edge absorption intensity. In conclusion, XANES measurements support the improvement of the ZnO crystal quality by annealing treatment observed from XRD measurements and suggest that incorporation of molecular oxygen during growth is responsible for the reduction in the crystal quality of non-stoichiometric samples with excess of oxygen.

4. Conclusions

ZnO thin films were grown by dc reactive magnetron sputtering at room temperature proving that this is a suitable technique in order to obtain ZnO coatings with good crystal and optical quality. After a previous optimization of the deposition parameters, we have obtained ZnO thin films with a controlled stoichiometry, good structural and morphological quality with the crystalline dimension normal to the *c*-axis, and optical properties (n and E_g) in good agreement with the reported values for stoichiometry ZnO bulk. A study of the bond structure by XANES of the annealed samples allows establishing a correlation between the excess of oxygen present in non-stoichiometric samples detected by RBS, and the degree of the crystallinity of the material. Furthermore, from these results it is possible to conclude that this excess of oxygen is incorporated as molecular oxygen, which produces the reduction of the crystallinity.

Acknowledgments

This work has been supported by the Ministerio de Ciencia e Innovación of (MICINN) of Spain through the Consolider-Ingenio 2010 programme (project FUNCOAT CSD2008-00023) and through project MAT2008-06618-C02-02/MAT. We are indebted to A Vollmer for her help at the Optics beamline (SURICAT endstation) of the Helmholtz-Zentrum Berlin - Electron storage ring BESSY II. The research leading to these results has received funding from the European Community's Seventh Framework Programme (FP7/2007-2013) under grant agreement no 226716. R Escobar Galindo and I Caretti acknowledge support from MICINN and CSIC through *Ramon y Cajal* (RyC2007-0026) and *JAE-Doc* fellowships, respectively.

References

[1] Fortunato E, Brida D, Ferreira I, Aguas H, Nunes P and Martins R 2001 *Thin Solid Films* **383** 310–13
[2] Lin L Y, Jeong M C, Kim D E and Myoung J M 2006 *Surf. Coat. Technol.* **201** 2547–52
[3] Berginski M, Hüpkes J, Schulte M, Schöpe G, Stiebig H, Rech B and Wuttig M 2007 *J. Appl. Phys.* **101** 074903-11
[4] Tvarozek V, Novotny I, Sutta P, Flickyngerova S, Schtereva K and Vavrinsky E 2007 *Thin Solid Films* **515** 8756–60
[5] Wang Z L 2004 *Mater. Today* **7** 26–33
[6] Fortunato E, Gonçalves A, Pimentel A, Barquinha P, Gonçalves G, Pereira L, Ferreira I and Martins R 2009 *Appl. Phys.* A **96** 197–205
[7] Carcia P F, McLean R S, Reilly M H, Crawford M K, Blanchard E N, Kattamis A Z and Wagner S 2007 *J. Appl. Phys.* **102** 074512
[8] Nanomarkets, 2011, Zinc Oxide Market Opportunities, http://nanomarkets.net/articles/article/zinc_oxide_market_opportunities
[9] Matsuia H and Tabata H 2005 *Appl. Phys. Lett.* **87** 143109
[10] Xua C X, Suna X W, Dongb Z L and Yuc M B J 2004 *Cryst. Growth* **270** 498–504
[11] Manzoor U and Kim D K 2009 *Physica* E **41** 500–5
[12] Zhang C 2010 *J. Phys. Chem. Solids* **71** 364–9
[13] Gabás M, Díaz-Carrasco P, Agulló -Rueda F, Herrero P, Landa-Cánovas A R and Ramos-Barrado J R 2011 *Sol. Energy Mater. Sol. Cells* **95** 2327–34
[14] Ho G W and Wong A S W 2007 *Appl. Phys.* A **86** 457–62
[15] Morgan J H and Brodie D E 1982 *Can. J. Phys.* **60** 1387–90
[16] Webb J B, Williams D F and Buchanan M 1981 *Appl. Phys. Lett.* **39** 640–2
[17] Mancini A M, Pierini P, Valentini A, Vasanelli L and Quirini A 1985 *Thin Solid Films* **124** 85–92
[18] Eberspacher C, Fahrenbruch A L and Bube R H 1986 *Thin Solid Films* **136** 1–10
[19] Anders A, Lim S H N , Yu K M, Andersson J, Rosén J, McFarland M and Brown J 2010 *Thin Solid Films* **518** 3313–9
[20] Ma Q B, Ye Z Z, He H P, Zhu L P and Zhao B H 2007 *Mater. Sci. Semicond. Process.* **10** 167–72
[21] Gao W and Li Z 2004 *Ceram. Int.* **30** 1155–9
[22] Singh S, Srinivasa R S and Major S S 2007 *Thin Solid Films* **515** 8718–22
[23] Zhu S, Su C H, Lehoczky S L, Peters P and George M A 2000 *J. Cryst. Growth* **211** 106–10
[24] Youssef S, Combette P, Podlecki J, Al Asmar R and Foucaran A 2009 *Cryst. Growth Des.* **9** 1088–94
[25] Mirica E, Kowach G, Evans P and Du H 2004 *Cryst. Growth Des.* **4** 157–9
[26] Gao Y and Nagai M 2006 *Langmuir* **22** 3936–40
[27] Song D, Aberle A G and Xia 2002 *Appl. Surf. Sci.* **195** 291–6
[28] Climent-Font A, Pászti F, García G, Fernández-Jiménez M T and Agulló F 2004 *Nucl. Instrum. Methods* B **219** 400–4
[29] Kotai E 1994 *Nucl. Instrum. Methods* B **85** 588–96
[30] CompleteEASE version 4.06 © 1999-2009 J.A. Woollam Co., Inc. http://www.jawoollam.com/completeease.html
[31] Forniés E, Escobar Galindo R, Sánchez O and Albella J M 2006 *Surf. Coat. Technol.* **200** 6047–53
[32] 2011 WebElements: the periodic table on the web, http://www.webelements.com
[33] Ellmer K, Klein A and Rech B 2008 *Transparent Conductive Zinc Oxide: Basics and Applications in Thin Film Solar Cells* (Berlin: Springer) p 212
[34] Washington P L, Ong H C, Dai J Y and Chang R P H 1998 *Appl. Phys. Lett* **72** 3261–3
[35] PCPDFWIN version 2.2 © 2001 JCPDS-ICDD http://www.icdd.com
[36] Lee Y C *et al* 2009 *J. Lumin.* **129** 148–52
[37] Kumar R, Khare N, Kumar V and Bhalla G L 2008 *Appl. Surf. Sci.* **254** 6509–13
[38] Zhu X and SakkaY 2008 *Sci. Technol. Adv. Mater.* **9** 033001
[39] Floro J A, Hearne S J, Hunter J A, Kotula P, Chason E, Seel S C and Thompson C V 2001 *J. Appl. Phys.* **89** 4886–97
[40] Chen J J, Gao Y, Zeng F, Li D M and Pa F 2004 *Appl. Surf. Sci.* **223** 318–29
[41] Movchan B A and Demchishin A V 1969 *Fiz. Met. Metalloved.* **28** 6653–60
[42] Thornton J A 1977 *Annu. Rev. Mater. Sci.* **7** 239–60
[43] Tompkins H G and McGahan W A 1999 *Spectroscopic Ellipsometry and Reflectometry* (New York: Wiley) p 93
[44] Paraguay D F, Estrada L W, Acosta N D R, Andrade E and Miki-Yoshida M 1999 *Thin Solid Films* **350** 192–202

[45] Li Q H, Zhu D, Liu W, Liu Y and Ma X C 2008 *Appl. Surf. Sci.* **254** 2922–6
[46] El Zawawi I K and Abd Alla R A 1999 *Thin Solid Films* **339** 314–9
[47] Tan S T, Chen B J, Sun X W, Fan W J, Kwok H S, Zhang X H and Chua X H 2005 *J. Appl. Phys.* **98** 013505
[48] Wu L, Wu Y and Lü W 2005 *Physica* E **28** 76–82
[49] Djouadi D, Chelouche A, Aksas A and Sebais M 2009 *Phys. Procedia* **2** 701–5
[50] Gupta P, Colvin V L and George S M 1988 *Phys. Rev.* B **37** 8234–43
[51] Vinnichenko M, Gago R, Cornelius S, Shevchenko N, Rogozin A, Kolitsch A, Munnik F and Möller W 2010 *Appl. Phys. Lett.* **96** 141907
[52] Singh A P, Kumar R, Thakur P, Brookes N B, Chae K H and Choi WK 2009 *J. Phys.: Condens. Matter* **21** 185005
[53] Persson C *et al* 2006 *Microelectr. J.* **37** 686–9
[54] Guo J H, Vayssieres L, Persson C, Ahuja R, Johansson B and Nordgren J 2002 *J. Phys.: Condens. Matter* **14** 6969–74
[55] Thakur P, Chae K H, Kim J Y, Subramanian M, Jayavel R and Asokan K 2007 *Appl. Phys. Lett.* **91** 162503
[56] Groot F M F, Grioni M, Fuggle J C, Ghijsen J, Sawatzky GA and Petersen H 1989 *Phys. Rev.* B **40** 5715–23
[57] Yan W, Sun Z, Liu Q, Li Z, Pan Z, Wang J, Wei S, Wang D, Zhou and Zhang X 2007 *Appl. Phys. Lett.* **91** 062113
[58] Outka D A, Stöhr J and Jark W 1987 *Phys. Rev.* B **35** 4119–22
[59] Kim C M, Jeong H S and Kim E H 2000 *Surf. Sci.* **459** 457–61
[60] Gago R, Jimenez I, Garcia I and Albella J M 2002 *Vacuum* **64** 199–204